Physics of Fluids

LETTER | NOVEMBER 01 2023

Acoustic driven circulation around cylindrical obstructions in microchannels

Md. Abdul Karim Miah ; Peter Zeller ; Michael G. Olsen ; Jaime J. Juárez

Check for updates

Physics of Fluids 35, 111701 (2023)
https://doi.org/10.1063/5.0172640

View Online
Export Citation
CrossMark

19 March 2024 15:40:09

AIP Publishing

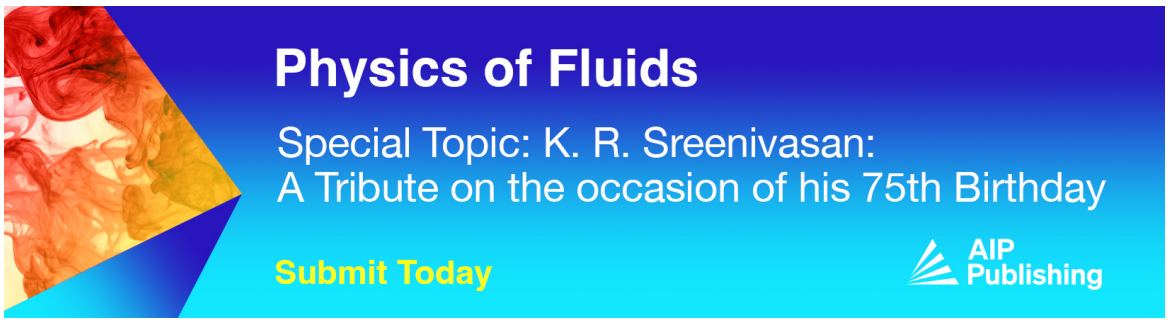

Physics of Fluids LETTER pubs.aip.org/aip/pof

Acoustic driven circulation around cylindrical obstructions in microchannels

Cite as: Phys. Fluids **35**, 111701 (2023); doi: 10.1063/5.0172640
Submitted: 17 August 2023 · Accepted: 15 October 2023 ·
Published Online: 1 November 2023

View Online Export Citation CrossMark

Md. Abdul Karim Miah, Peter Zeller, Michael G. Olsen,[a] and Jaime J. Juárez[a]

AFFILIATIONS

Department of Mechanical Engineering, Iowa State University, Ames, Iowa 50011, USA

[a]Authors to whom correspondence should be addressed: mgolsen@iastate.edu and jjuarez@iastate.edu

ABSTRACT

We introduce an approach to generate direction-controlled circulation around cylindrical obstructions in channels using a piezoelectric transducer embedded porous-channel device fabricated by photolithography. To transmit acoustic signals into the channel, a single piezoelectric transducer was attached, operating at voltage levels of 5, 10, 15, and 20 V. Microscopic particle image velocimetry was employed to analyze the flow patterns in the channels. The analysis revealed two opposing circulation tendencies around the pillars located at two opposite sides of the channel in the longitudinal direction. The strength of circulation was found to be minimal in the middle of the channel and increased gradually toward the two ends of the channels. Furthermore, we observed that the circulation strength was maximum near the axial centerline and minimum at the boundaries along the width of the channels. Comparing the voltage levels, the higher voltage signals produced a higher strength of circulation than the lower voltage signals in all cases. Additionally, we found that the strength of circulation increased almost linearly and then decayed exponentially in the radial direction from the surfaces of the pillars. The observed velocity fields around individual cylinders matched well with the Görtler vortex model. The reported circulation phenomenon around pillars can be applied in non-contact fluid stirring and mixing in bio-chemical systems and lab-on-a-chip systems and may also provide additional degrees of freedom in object tweezing, trapping, and levitation.

Published under an exclusive license by AIP Publishing. https://doi.org/10.1063/5.0172640

19 March 2024 15:40:09

Acoustic streaming plays a crucial role in various applications such as particle sorting,[1] fluid mixing,[2] and heat transfer.[3] This mechanism results from the dissipation of acoustic energy in the fluid that creates a body force that generates bulk flow.[4] More recently, it has been determined that acoustic field interactions with obstacles or boundaries within microfluidic devices can form complex secondary flows,[5] which has implications for precise particle manipulation,[6] improved microscale propulsion[7] or enhanced oil recovery.[8] Process control of these complex flows is challenging as they depend on factors such as obstacle geometry, fluid properties, and acoustic wave characteristics.[9] Thus, there is a need to characterize acoustic streaming behavior in the presence of obstacles.

In this investigation, we present microscopic particle image velocimetry (μPIV) measurements of direction-controlled circulation modulated by acoustic streaming. Although there are reports of acoustic streaming about sharp obstacles,[5] this work demonstrates that flow patterns are also generated about cylindrical obstacles located in a microchannel. The circulation intensity around these obstacles is dependent on applied voltage and relative location (i.e., distance and angle) from the acoustic source. The circulation rate is minimal near the axial midpoint of the device, near where the acoustic source is located, and increases moving away from the center toward the device inlet and outlet. Comparing the measured velocities to several analytical models indicates that the circulation pattern appears to match the Görtler vortex model. This circulation phenomenon has the potential to be used in fluid stirring and mixing, lab-on-a-chip systems, object manipulation, levitation, trapping, and tweezing.

The microfluidic device used to investigate the acoustically generated circulation is shown in Fig. 1. Two separate geometries were used in experiments. The first design consists of a series of cylindrical obstacles with a porosity of ~92%. As a control, we also fabricated an open channel without obstacles. Both channels were 17 mm in length, 2 mm in width, 50 μm in depth, and contained 4 mm diameter inlet and outlet reservoirs. The porous channel also contained an array of cylindrical pillars of 150 μm diameter. The channels were fabricated with polydimethylsiloxane (PDMS) using lithography and were bonded to a cover glass with dimensions of $48 \times 65\,\text{mm}^2$ following plasma cleaning. A 27 mm diameter piezoelectric transducer (PZT) served as an acoustic source (Digi-Key, product # 668-1407-ND) with manufacturer-reported unloaded resonant frequency of 4.6 kHz.

Published under an exclusive license by AIP Publishing

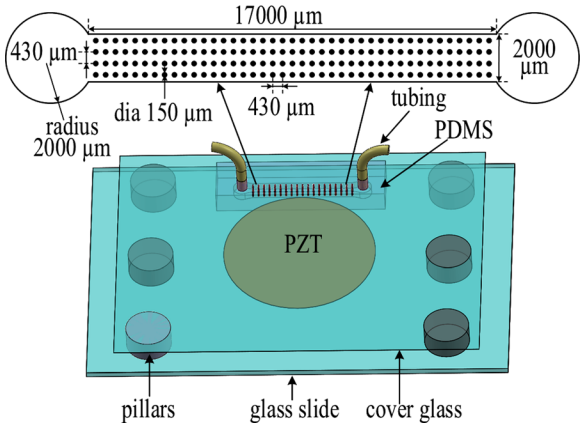

FIG. 1. The microfluidic device used in the experiment. A PZT is attached underneath the cover glass on which the channel is bonded. Six silicone pillars support the device. The inset above displays the channel's dimensions.

The PZT was attached underneath the cover glass and positioned as close to the channel center as possible. The device sits on six silicone pillars with heights of 3.8 mm, each. The pillars are glued to a microscope slide with dimensions $75 \times 50 \times 1$ mm^3. The assembled device is shown in Fig. 1.

An Olympus IX70 microscope was used for fluorescence microscopy with a 4× magnification (0.1 NA) objective and a 10× (0.3 NA) objective. An LED fluorescence light source (X-Cite Fluorescence Lamp, Model No. XT640-W) served as an illumination source. One micrometer diameter fluorescent polystyrene particles (Thermo Fisher Scientific, product # F8852) were used as tracer particles. A particle dispersion was prepared using 120 μl of the particle stock solution, which was added to 3 ml of de-ionized water. Prior to use, the dispersion was sonicated for 5 min. The fluorescent particles have excitation/emission peaks at 505/515 nm. A function generator (Tektronix AFG1022) was used to drive the PZT at four voltage levels and at different frequencies. The signal was amplified with an RF amplifier (Amplifier Research Model 50A220). A Tektronix TBS 1052B-EDU oscilloscope was used to confirm the applied signal frequency and amplitude. A 2.3 megapixel monochrome camera (1920 × 1200 pixels) from Teledyne FLIR (model no. GS3-U3–23S6M-C) was used for recording video from the microscope. The camera captured images at ~160 fps.

The captured images were analyzed using an open-source μPIV analysis software known as PIVLab.[10] This software relies on the discrete Fourier transform algorithm to calculate velocity fields using the cross correlation approach.[11,12] The spatial resolution of the measurements was maximized by performing multiple passes with various sized interrogation areas. Since the experimentally generated flow field was steady, an ensemble-averaged correlation was used to maximize the vector resolution. For each experiment, 750 images were taken. The in-plane spatial resolution for the experiments in the porous channel was 27.8 μm for the 10× measurements and 33.4 μm for the 4× measurements, respectively. The in-plane spatial resolution for the open channel was 111 μm for the 4× measurements. The out-of-plane spatial resolution (or depth of correlation) was 25 μm for the 10× measurements, and the out-of-plane spatial resolutions spanned the entire depth for the 4× measurements.[13–15]

The experiments were conducted by introducing an acoustic signal in the quiescent water phase in both the open channel and 92% porosity channel. Fluid circulation was observed in the channels when subjected to peak-to-peak voltages of 5, 10, 15, and 20 V at a loaded resonance frequency of 5.2 kHz. The vortex intensity was found to be highest at this resonance frequency for both channel types. No circulation was observed below 4.6 kHz and above 6.4 kHz. Circulation was observed within this frequency range, with the maximum circulation occurring at 5.2 kHz. For the porous channel, images and corresponding velocity fields were captured at five channel locations: center (i.e., directly opposite the PZT), right, far right, left, and far left using a 4× magnification, as shown in Fig. 2. The right and left windows are positioned at 3 mm distance from the center of the channel, while the far right and far left windows are positioned at 7.45 mm distance from the channel center. To obtain a magnified view of the vortex phenomena around the cylindrical obstructions, images were taken at two locations at a higher magnification using 10× magnification, and the results are depicted in Fig. 3. In the case of the open channel, four measurement positions were chosen: right, left, far right, and far left from the channel's center. The right and left windows are positioned at 2.7 mm distance from the center of the channel, while the far right and far left windows are positioned at 6.2 mm distance from the channel center. The center position was excluded as no circulation was observed at this location.

In the porous channel, circulation was observed around each of the cylindrical pillars, as shown in Fig. 2. The pillars to the right of the PZT displayed clockwise circulation, whereas the pillars to the left showed counterclockwise circulation. Velocities were zero in the space between cylinders, indicating no induced bulk fluid motion in the channels apart from the circulation around the cylinders. For the different longitudinal locations, the circulation strength was smallest at the center location, and it increased moving away from the center toward the left or right sides. In the transverse direction, the circulation intensity was lowest around the pillars closest to the microchannel walls and greatest around cylinders near the middle of the channel. Higher voltage inputs induce an increased circulation intensity. The data shown in Fig. 2 exhibit a maximum velocity measured at 20 V that is 3.8 times greater than the maximum velocity measured at 10 V. We derive a scaling relationship between voltage and velocity by examining the characteristic acoustic velocity amplitude, $u_o = 4E_{ac}/Z_o$, where E_{ac} is the acoustic energy density, and Z_o is the acoustic impedance of the fluid.[16] A scaling analysis of acoustic interactions in microchannels shows that E_{ac} scales quadratically with applied voltage ($E_{ac} \propto V_{app}^2$).[17] Thus, based on this observation, we surmise that $u_o \propto V_{app}^2$, which explains the nearly factor of 4 increase in velocity when voltage is doubled. This quadratic scaling relationship holds across four different voltages (5, 10, 15, and 20 V) as illustrated by Fig. S1 in supplementary material.

Figure 2 represents a wide view of the acoustically driven circulation phenomena. The view allowed us to observe that circulation around the pillars exhibits a slightly elliptical shape aligned at a 45-degree angle with respect to the longitudinal axis. Moving longitudinally away from the center, the slightly elliptical profile gradually transforms into a circular profile. Notably, the circulation profiles on the left and right sides of the channel were mirror images of each other. We obtained a focused view of circulation using 10× magnification in Fig. 3, where the results for 10 and 20 V circulation around individual

19 March 2024 15:40:09

Published under an exclusive license by AIP Publishing

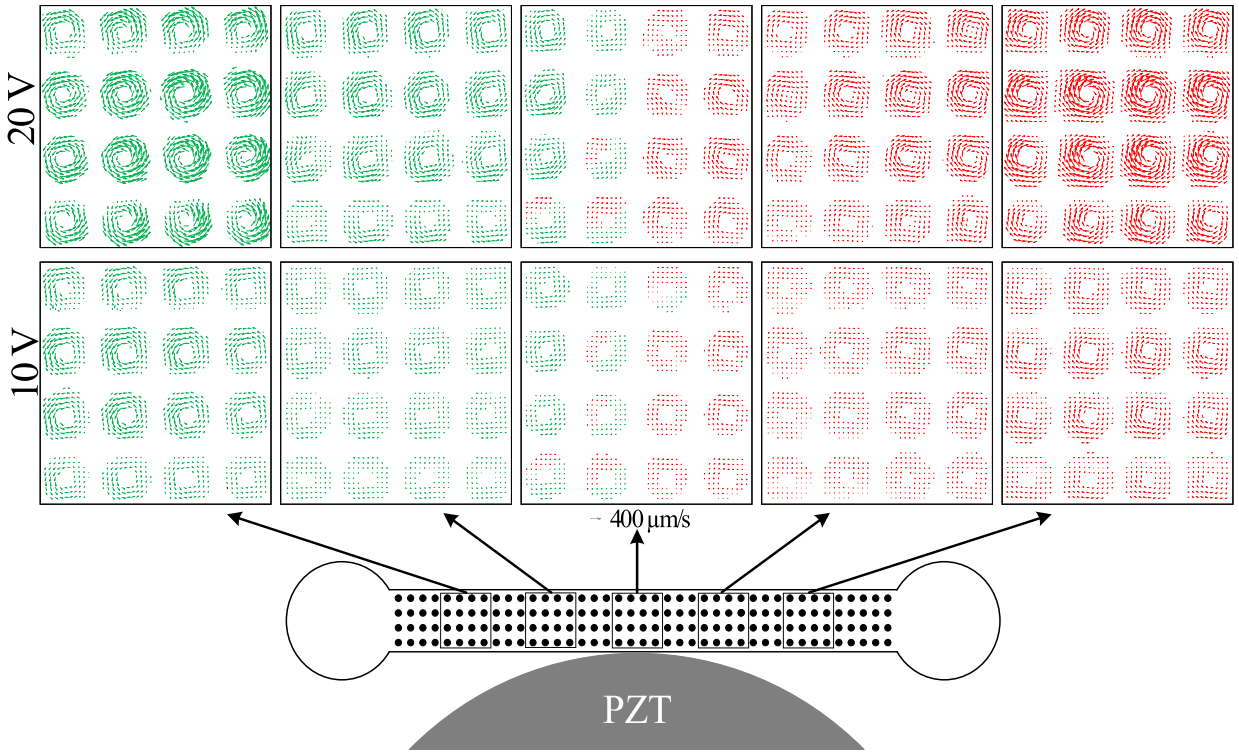

FIG. 2. Measured velocity fields at five different positions in the porous channel for 10 and 20 V acoustic signals at 5.2 kHz. Images were captured at 4× magnification. Circulation is counterclockwise (green color) on the left and clockwise (red color) on the right.

cylinders are shown at the far left and far right positions of the porous channel. The circulation velocity is highest close to the pillar surface and decays moving away from the pillar surface. The acoustic pressure distribution around the pillars can be inferred from the expression of Barnkob *et al.*,[17] $P_a = 2\sqrt{Z_o c_f E_{ac}}$. Utilizing the previously mentioned relationship between velocity and acoustic energy density, we find that the relationship between acoustic pressure and velocity is $P_a = Z_o\sqrt{c_f u_o}$. The acoustic pressure distribution, shown in Figs. S2 and S3, illustrates that the acoustic pressure is strongest near the pillar surface. This indicates that they act as transmission points, through which the acoustic wave generated by the PZT interacts with the surrounding fluid. This leads to the circulation behavior observed in our μPIV results. The peak acoustic pressure observed in this analysis is plotted in Fig. S4 as a function of voltage. The figure shows that acoustic pressure scales linearly with voltage, which is expected if velocity scales quadratically and pressure relates to velocity by a square root term.

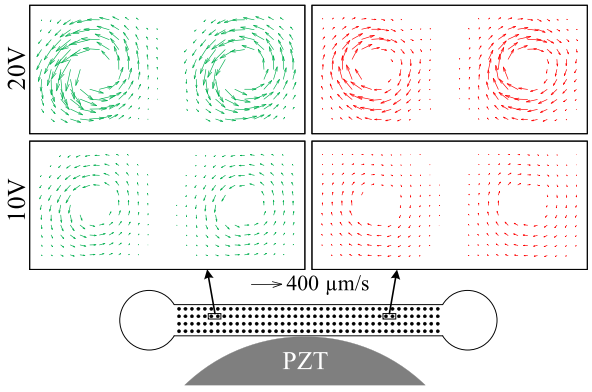

FIG. 3. Measured velocity fields around individual cylinders near the two ends of porous channel for 10 and 20 V acoustic signals at 5.2 kHz. Images were captured at 10× magnification. Circulation is counterclockwise (green color) on the left and clockwise (red color) on the right.

For comparison, velocity fields at four positions in the open channel for 10 and 20 V acoustic signals are presented in Fig. 4. In contrast with the case of the porous channel, no circulation was observed at the middle location. Bulk fluid circulation spanning the entire width of the channel in the clockwise direction was found at the two positions to the right of the channel center, and similar counterclockwise circulation was observed at the two positions to the left of the channel center. The circulation strength of the bulk circulations situated farthest from the center showed higher values than the circulations that are closer to the center. The peak velocities in these bulk vortices are considerably smaller than the peak velocities in the vortices observed around the cylindrical pillars in the porous microchannel, with the circulation velocities around the cylindrical pillars approximately 3.65 times greater than the bulk circulation velocities. Note that the presence of the cylindrical pillars in the porous channel appears to completely

19 March 2024 15:40:09

Published under an exclusive license by AIP Publishing

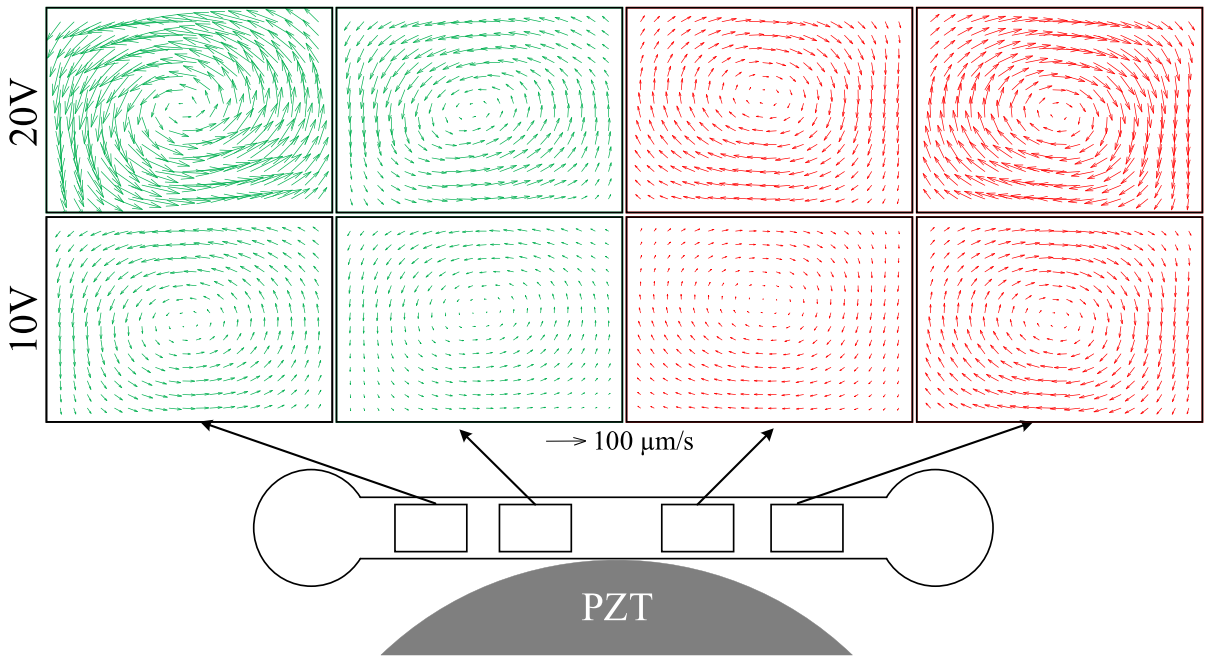

FIG. 4. Measured velocity fields at four different positions in the open channel for 10 and 20 V acoustic signals at 5.2 kHz. Images were captured at 4× magnification. Circulation is counterclockwise (green color) on the left and clockwise (red color) on the right.

disrupt the formation of bulk, channel-width spanning circulation, as in the porous case the circulation is only observed around the individual pillars.

Figure 5 shows the tangential velocity as a function of radial distance for the flow around a cylindrical pillar at the far-left location for an acoustic signal of 5, 10, 15, and 20 V at 5.2 kHz. The profile exhibits a quasi-linear increase and then a decay of the tangential velocity with increasing radial distance from the pillar surface. The experimentally measured velocity profile was compared with velocity profiles predicted by four theoretical vortex models: the Görtler,[18–20] Lamb–Oseen,[21] Rankine,[18,22] and Vatistas[23–26] vortex models. The Lamb–Oseen model, Rankine model, and Vatistas model were found to deviate significantly from experimental results. For all voltage levels, the Görtler model is found to best describe acoustically driven circulation around the cylindrical pillar. In Fig. 5, the comparison of experimental velocity profile and the velocity profile predicted by Görtler model has been presented.

In cylindrical coordinates, the tangential velocity distribution in Görtler vortices is[20]

$$v_\theta(r) = C\left(\frac{Z_0^2}{Z^2}\right)\frac{2(r/r_0)}{\left[1 + r^2/r_0^2\right]^2}, \tag{1}$$

where C is a constant obtained from the vorticity distribution at location Z_0 in the z (out-of-plane) coordinate, and the length scale r_0 is a boundary layer thickness. Our experiments were conducted in a thin channel (50 μm); thus, we assume that $Z_0^2/Z^2 \approx 1$, which reduces Eq. (1) to

$$v_\theta(r) = C\frac{2(r/r_0)}{\left[1 + r^2/r_0^2\right]^2}. \tag{2}$$

Equation (2) was fit to the decaying component of the tangential velocity data shown in Fig. 5. The curve fit was performed using C and r_o as free parameters. The parameters obtained through this fitting process are shown in Table I. Plotting the parameter, C, as a function of voltage in Fig. S5(a), we observe that $C \propto V_{app}^{1.72}$, which is close to the quadratic scaling predicted by our analysis above. This discrepancy in scaling can be attributed to the other fitting parameter in the Görtler model, r_o, which exhibits a slight linear dependence on voltage as shown in Fig. S5(b).

Scaling models for acoustic boundary layers in an open channel suggest that $r_0 \approx \sqrt{2\nu/\omega}$, where ν is the fluid kinematic viscosity, and ω is the angular frequency of oscillation.[27] For water oscillating at 5.2 kHz, this scaling model suggests that that the boundary layer should be 7.8 μm. However, this is larger than the values estimated from Table I. The discrepancy is likely associated with the open channel assumption. Our device consists of multiple obstacles, with rotation observed around each obstacle (and hence, the boundary layers forming around the cylindrical obstacles and not straight channel walls). The hydrodynamic interactions of the rotation superimposed on each other may impact the decay length of the acoustic signal. Furthermore, the acoustic signal is likely dampened by passing through the constituent components of our device (i.e., glass, PDMS, and water), an effect that is not captured by the boundary layer thickness model.

In summary, the authors investigated induced circulatory motion in a microfluidic channel containing cylindrical obstacles acoustically actuated by a piezoelectric transducer (PZT). The induced circulation around the cylinders was observed to vary in both the transverse and longitudinal directions, with opposing direction of circulation on either side of the PZT. The radial

19 March 2024 15:40:09

Published under an exclusive license by AIP Publishing

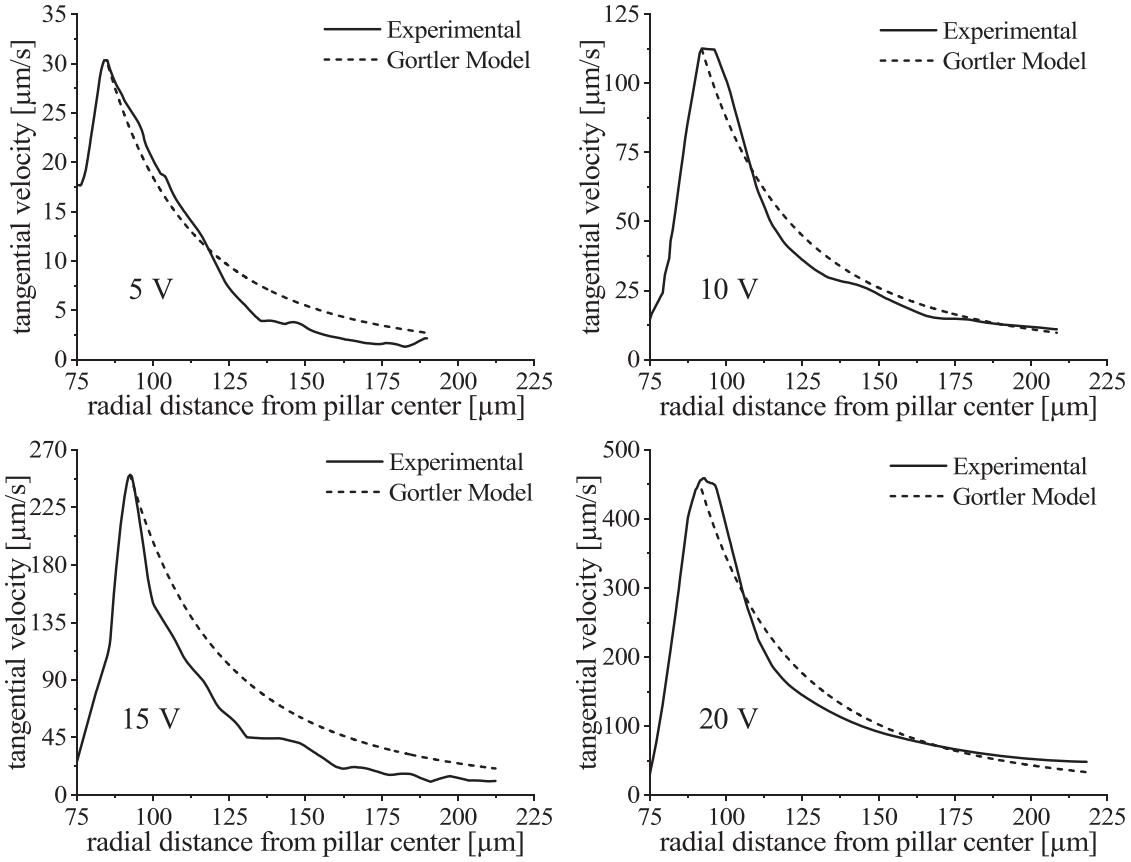

FIG. 5. Profiles of tangential velocity as a function of radial distance from the cylindrical pillar center for the far left position at 5 V (top left), 10 V (top right), 15 V (bottom left), and 20 V (bottom right), 5.2 kHz excitation, in comparison with the Görtler model.

TABLE I. Fitting parameters for the Görtler model [Eq. (2)] obtained from analysis of circulation data at 5, 10, 15, and 20 V.

	Applied voltage			
Görtler fitting parameters	5 V	10 V	15 V	20 V
$\frac{C}{10^6}$ (μm/s)	1.73	6.55	13.4	17.78
r_o (μm)	1.75	1.88	1.95	2.13

profile of tangential velocity around the cylinders was consistent with the Görtler vortex model. The boundary layer thickness observed in the experiment is different from what is expected by scaling models. This is likely the result of a combination of hydrodynamic interactions within the micromodel and acoustic signal impedance. This acoustic-induced circulation has an array of potential applications, including non-intrusive fluid stirring and mixing in biological and chemical systems, lab-on-a-chip systems, manipulation of micro- and nanoparticles, and mid-air object levitation. This phenomenon may also provide additional degrees of freedom for acoustic tweezing, trapping, and object manipulation.

SUPPLEMENTARY MATERIAL

See the supplementary material for details on acoustic pressure and velocity relationships as a function of voltage; a graph describing the impact that voltage has on the Görtler model; measurement of pillar uniformity; and goodness of fit for the vortex circulation models considered in this paper.

The authors gratefully acknowledge the financial support from the National Science Foundation under Grant No. 2050105.

AUTHOR DECLARATIONS

Conflict of Interest

The authors have no conflicts to disclose.

Author Contributions

Md. Abdul Karim Miah: Data curation (equal); Formal analysis (equal); Investigation (equal); Methodology (equal); Software (equal); Validation (equal); Visualization (equal); Writing – original draft (equal). **Peter Zeller:** Data curation (equal); Formal analysis (equal); Investigation (equal); Methodology (equal); Software (equal); Validation (equal); Visualization (equal); Writing – original draft (equal). **Michael G. Olsen:**

19 March 2024 15:40:09

Published under an exclusive license by AIP Publishing

Conceptualization (equal); Data curation (equal); Funding acquisition (equal); Investigation (equal); Methodology (equal); Project administration (equal); Resources (equal); Writing – review & editing (equal). **Jaime J. Juarez:** Conceptualization (equal); Data curation (equal); Funding acquisition (equal); Methodology (equal); Project administration (equal); Resources (equal); Supervision (equal); Writing – review & editing (equal).

DATA AVAILABILITY

The data that support the findings of this study are available from the corresponding authors upon reasonable request.

REFERENCES

[1]J. W. Ng, D. J. Collins, C. Devendran, Y. Ai, and A. Neild, "Flow-rate-insensitive deterministic particle sorting using a combination of travelling and standing surface acoustic waves," Microfluid. Nanofluid. **20**(11), 151 (2016).

[2]D. Ahmed, X. Mao, B. K. Juluri, and T. J. Huang, "A fast microfluidic mixer based on acoustically driven sidewall-trapped microbubbles," Microfluid. Nanofluid. **7**(5), 727 (2009).

[3]P. Vainshtein, M. Fichman, and C. Gutfinger, "Acoustic enhancement of heat transfer between two parallel plates," Int. J. Heat Mass Transfer **38**(10), 1893–1899 (1995).

[4]H. Lei, D. Henry, and H. BenHadid, "Acoustic force model for the fluid flow under standing waves," Appl. Acoust. **72**(10), 754–759 (2011).

[5]Z. Chen, P. Liu, X. Zhao, L. Huang, Y. Xiao, Y. Zhang, J. Zhang, and N. Hao, "Sharp-edge acoustic microfluidics: Principles, structures, and applications," Appl. Mater. Today **25**, 101239 (2021).

[6]Z. Ma, Y. Zhou, F. Cai, L. Meng, H. Zheng, and Y. Ai, "Ultrasonic microstreaming for complex-trajectory transport and rotation of single particles and cells," Lab Chip **20**(16), 2947–2953 (2020).

[7]F.-W. Liu and S. K. Cho, "3-D swimming microdrone powered by acoustic bubbles," Lab Chip **21**(2), 355–364 (2021).

[8]H.-L. Yeh and J. J. Juárez, "Oil phase displacement by acoustic streaming in a reservoir-on-a-chip," Microfluid. Nanofluid. **23**(10), 113 (2019).

[9]S. J. Lighthill, "Acoustic streaming," J. Sound Vib. **61**(3), 391–418 (1978).

[10]W. Thielicke and R. Sonntag, "Particle Image Velocimetry for MATLAB: Accuracy and enhanced algorithms in PIVlab," J. Open Res. Software **9**(1), 12 (2021).

[11]M. Raffel, C. E. Willert, S. T. Wereley, and J. Kompenhans, *Particle Image Velocimetry: A Practical Guide* (Springer, Berlin, Heidelberg, 2007).

[12]J. Westerweel, "Fundamentals of digital particle image velocimetry," Meas. Sci. Technol. **8**(12), 1379 (1997).

[13]C. J. Bourdon, M. G. Olsen, and A. D. Gorby, "Power-filter technique for modifying depth of correlation in microPIV experiments," Exp. Fluids **37**(2), 263–271 (2004).

[14]C. J. Bourdon, M. G. Olsen, and A. D. Gorby, "Validation of an analytical solution for depth of correlation in microscopic particle image velocimetry," Meas. Sci. Technol. **15**(2), 318 (2004).

[15]M. G. Olsen and R. J. Adrian, "Out-of-focus effects on particle image visibility and correlation in microscopic particle image velocimetry," Exp. Fluids **29**(1), S166–S174 (2000).

[16]R. Barnkob, P. Augustsson, T. Laurell, and H. Bruus, "Acoustic radiation- and streaming-induced microparticle velocities determined by microparticle image velocimetry in an ultrasound symmetry plane," Phys. Rev. E **86**(5), 056307 (2012).

[17]R. Barnkob, P. Augustsson, T. Laurell, and H. Bruus, "Measuring the local pressure amplitude in microchannel acoustophoresis," Lab Chip **10**(5), 563–570 (2010).

[18]S. Rodriguez, F. Espinoza, S. Steinberg, and M. El-Genk, "Towards a unified swirl vortex model," AIAA Paper No. 2012-3354, 2012.

[19]H. Görtler, "Decay of swirl in an axially symmetrical jet, far from the orifice," Rev. Mat. Hisp.-Am. **14**(4–5), 143–178 (1954).

[20]M. R. Khorrami, "Stability of a compressible axisymmetric swirling jet," AIAA J. **33**(4), 650–658 (1995).

[21]J. W. Batterson, B. A. Maicke, and J. Majdalani, *Advancements in Theoretical Models of Confined Vortex Flowfields* (Defense Technical Information Center, University of Tennessee Space Institute, TN, 2007).

[22]T. Gerz, F. Holzäpfel, and D. Darracq, "Commercial aircraft wake vortices," Prog. Aerosp. Sci. **38**(3), 181–208 (2002).

[23]A. Povitsky, T. Zheng, and G. H. Vatistas, "Effect of vortex profile on sound generation in a non-uniform flow," Math. Comput. Simul. **65**, 447–468 (2004).

[24]G. H. Vatistas, "New model for intense self-similar vortices," J. Propul. Power **14**(4), 462–469 (1998).

[25]G. H. Vatistas, V. Kozel, and W. C. Mih, "A simpler model for concentrated vortices," Exp. Fluids **11**(1), 73–76 (1991).

[26]N. A. R. Nik Mohd and G. N. Barakos, "Computational aerodynamics of hovering helicopter rotors," J. Mek. **34**, 16–46 (2012), https://jurnalmekanikal.utm.my/index.php/jurnalmekanikal/article/view/76.

[27]H. Bruus, "Acoustofluidics 7: The acoustic radiation force on small particles," Lab Chip **12**(6), 1014–1021 (2012).

19 March 2024 15:40:09

Published under an exclusive license by AIP Publishing